Identification of a Cd^{2+}- and Zn^{2+}-Binding Site in Cytochrome *c* Using FTIR Coupled to an ATR Microdialysis Setup and NMR Spectroscopy†

Samuel Gourion-Arsiquaud,‡ Soizic Chevance,§ Pierre Bouyer,‡ Lionel Garnier,|| J.-L. Montillet,|| Arnaud Bondon,*,§ and Catherine Berthomieu*,‡

Laboratoire de Bioénergétique Cellulaire, CEA/Cadarache, DSV-DEVM, UMR 6191 CNRS-CEA-Université Aix-Marseille II, F-13108 Saint-Paul-lez-Durance, Cedex, France, RMN-Interactions Lipides Protéines, UMR CNRS 6026, Campus de Villejean, CS 34317, Université de Rennes 1, 35043 Rennes Cedex, France, and Laboratoire de Radiobiologie Végétale, CEA/Cadarache, DSV-DEVM, F-13108 Saint-Paul-lez-Durance, Cedex, France

Received February 21, 2005; Revised Manuscript Received May 2, 2005

ABSTRACT: Fourier transform infrared (FTIR) difference spectroscopy allows the study of molecular changes occurring at active sites in proteins with high sensitivity. Reactions are triggered by light, potential, or temperature steps and more recently by the diffusion of buffers containing effectors above membrane proteins deposited as films on ATR crystals. We have adapted a microdialysis system to an ATR, to study metal sites in soluble proteins. In this study, we identified a Cd^{2+}- or Zn^{2+}-binding site in cytochrome *c* with dissociation constants of 17 and 42 μM, respectively, which affects the oxidation rate of ferrocytochrome *c* by hydrogen peroxide. Using the microdialysis ATR−FTIR setup, we determined that a histidine and the carboxylate group of a glutamate are involved in Zn^{2+} binding. The implication of His 33 and Glu 104 in the binding site was deduced from the comparison of FTIR data recorded with horse heart and the variant tuna cytochrome *c* lacking these two amino acids. A two-dimensional NMR analysis of the Zn^{2+}-binding site in horse heart cytochrome *c* confirmed that His 33 and residues close to the C terminus are sensitive to Zn^{2+} binding. This study demonstrates that the microdialysis ATR−FTIR setup is promising for the analysis of metal sites in proteins. From $H_2O/^2H_2O$ exchange experiments, we concluded that the impact of Zn^{2+} and Cd^{2+} binding on the oxidation kinetics of ferrocytochrome *c* by H_2O_2 is associated to the perturbation of a hydrogen-bonding network involving His 33 that is sensitive to the redox state of cytochrome *c*.

Besides their vital function in organisms, metals are involved in pathogenic processes through various mechanisms, such as production of reactive oxygen species, alteration of the redox balance in the cytoplasm, and direct interactions with DNA, RNA, and proteins (*1*, *2*). Toxicity results from the exposition to nonbiological metals and from direct or indirect alteration of metal homeostasis in the cell. Metal trafficking is highly regulated. It involves metal-binding proteins with various functions, transporters, chaperones for the delivery of essential metals to target metalloenzymes, metal-sensitive transcription regulators, and proteins that ensure the chelation and sequestration of toxic metals (*3*, *4*). To analyze these processes, growing attention is devoted to the identification and characterization of metal-binding sites in proteins and of structural parameters governing metal affinity and specificity.

Metal ligands are determined from three-dimensional structures, obtained using X-rays diffraction on crystals or nuclear magnetic resonance (NMR)[1] spectroscopy. For proteins and protein motifs that are not accessible to these techniques or to rapidly probe the properties of metal sites, methods derived from electron paramagnetic resonance (EPR), magnetic circular dichroism, Mössbauer, and X-ray absorption spectroscopy have proven useful. They provide information on the geometry and electronic properties of the metal sites (*5*−*7*). They apply however to metal sites with particular properties and do not always provide information on the nature of the amino acid ligands.

The metal ligands and structural changes associated with metal binding can be identified using NMR spectroscopy for paramagnetic species (*7*) or for proteins for which the full NMR assignment of the protons is available. In the absence of drastic structural changes of the protein after metal binding, this technique is powerful for the rapid determination of residues involved in the metal-binding site.

† S.G.-A. acknowledges a Ph.D. fellowship from the Commissariat à l'Energie Atomique and the Provence Alpes Côte d'Azur region. This work was supported in part by the French Program Toxicologie Nucléaire Environnementale.

* To whom correspondence should be addressed. Telephone: 33 (0)4 42 25 43 53. fax 33 (0) 4 42 25 47 01. E-mail: catherine.berthomieu@cea.fr (C.B.); Telephone: 33 (0)2 23 23 65 61. Fax: 33 (0)2 23 23 46 06. E-mail: arnaud.bondon@univ-rennes1.fr (A.B.).

‡ Laboratoire de Bioénergétique Cellulaire.

§ Université de Rennes 1.

|| Laboratoire de Radiobiologie Végétale.

[1] Abbreviations: (ferro)cyt *c*, (ferro)cytochrome *c*; EPR, electron paramagnetic resonance; FTIR, Fourier transform infrared; ATR, attenuated total reflection; IRE, internal reflection element of the ATR; NMR, nuclear magnetic resonance; HSQC, heteronuclear single-quantum correlation; TPPI, time proportional phase incrementation; Tris, Tris-hydroxymethyl-aminomethane; TMPD, *N*,*N*,*N*′,*N*′-tetramethyl-paraphenylene-diamine.

10.1021/bi050322l CCC: $30.25
Published on Web 05/27/2005

Vibrational spectroscopy is also particularly useful, both to identify the chemical groups involved in metal binding and to analyze the properties of the metal−ligand interactions. (Resonance) Raman spectroscopy has long been applied to metal sites absorbing in the visible or near-infrared range (*8*). This excludes certain metal oxidation states or metal centers and often Zn^{2+}- or Cd^{2+}-binding sites. As for UV−Raman, which probes amino acids absorbing in the UV range, it is a valuable tool to characterize histidines coordinated to Zn or Cu (*9*, *10*). Infrared spectroscopy, which probes directly the vibrational transitions of molecules, also describes the electronic properties of the amino acid ligands of the metal. An advantage of IR spectroscopy is that it can be applied in principle to all kinds of metals, diamagnetic to very paramagnetic, all redox states, and proteins that are not accessible to other spectroscopic techniques such as NMR or X-ray diffraction on crystals.

The strong infrared absorption of water and of the protein backbone prevents however the analysis of metal-binding sites directly from the sample infrared absorption. Over the past decade, Fourier transform infrared (FTIR) difference spectroscopy considerably developed for the analysis of fine structural changes at active sites in proteins. Light-induced FTIR difference spectroscopy has given valuable information on light-sensitive proteins such as bacteriorhodopsin or photosynthetic reaction centers (*11*−*15*). Implementation of photoactivable caged compounds and of a specific electrochemical cell largely extended the application of this technique (*16*−*18*). A decisive development for generalizing FTIR difference spectroscopy to study membrane proteins was the use of attenuated total reflection (ATR; *19*, *20*). This approach takes advantage of the deposition of the membrane protein as a stable layer on the ATR crystal surface, which is probed by the infrared beam, while addition of effectors is performed above the layer, without consequence on the quality of the FTIR difference spectra. With this setup, structural changes induced by the binding of ligands or agonists on nicotinic acetylcholine receptors (*21*, *22*) or of inhibitors in cytochrome *c* oxidase and in the bc_1 complex (*23*−*26*) were analyzed at the molecular level. H/^{2}H exchange experiments were also performed, by diffusion of H_2O/^2H_2O-saturated N_2 flux, to describe conformational changes induced by phosphorylation or the binding of ligands (*27* and references therein).

A dialysis system was introduced by K. Fahmy (*28*, *29*) to analyze changes in secondary structures of rhodopsin within the membrane, induced by the binding of transducin. To our knowledge, up to now, no information has been obtained at the molecular level, for proteins in solution, directly using the perfusion of effectors through a dialysis system.

In the following, we describe a new application of ATR−FTIR spectroscopy based on the use of a microdialysis system adapted to an ATR cell, to analyze molecular details on proteins in solution, directly by the perfusion of effectors or redox compounds. The present work demonstrates the efficiency of this method to analyze both redox reactions or metal-binding sites in proteins, using cytochrome *c* (cyt *c*) and a comparison of the IR data with results obtained with NMR spectroscopy. One very attractive interest of this ATR−FTIR approach will be to study membrane proteins such as metal transporters, which are not easily accessible by NMR.

Cyt *c* is one of the most abundant proteins in mitochondria. It is closely associated to the mitochondria membrane and mediates electron shuttling between ubiquinol−cytochrome *c* oxidoreductase and cytochrome *c* oxidase during respiration (*30*). Cyt *c* dissociation from the mitochondria membrane is associated with early events leading to apoptosis (*31*, *32*). Therefore, because of its small size, the availability of its structure, and its structural plasticity, cyt *c* has served as a model for the analysis of intra- and inter-electron transfer and for the mechanisms of folding and protein−protein or protein−lipid association (*33*−*39*). Structural data and NMR resonance assignment of all amino acid contributions have allowed the analysis of structural changes induced by ionic strength (*40*, *41*) or insertion in micelles (*36*, *42*). The consequences of cyt *c* association with surface-modified electrodes were also studied by electrochemistry and Raman or FTIR spectroscopy (*43*, *44*).

The mechanisms of cyt *c* dissociation from the mitochondria membrane is a field of intense research. Cyt *c* is proposed to play a key role as a peroxidase that reacts with hydrogen peroxide to oxidize mitochondrial phospholipids thus initiating apoptosis (*32*, *45*−*47* and references therein). The mitochondrial electron transport chain is a main source of reactive oxygen species (*48*), which could promote the release of cyt *c* from the mitochondria (*49*), through the oxidation of cyt *c* associated cardiolipin (*50*). While H_2O_2 slowly oxidizes reduced cyt *c* (ferrocyt *c*) in solution (*51*), cyt *c* reactivity toward H_2O_2 is greatly enhanced upon association with phosphatydilserine or cardiolipin (*32*).

In this work, we report that Zn^{2+} and Cd^{2+} strongly and selectively slow the oxidation kinetics of ferrocyt *c* monitored by H_2O_2. Using the ATR−FTIR microdialysis setup and NMR spectroscopy, we identify a binding site for Zn^{2+} or Cd^{2+} that involves His 33 and Glu 104 at the C terminus. The mechanisms by which Zn^{2+} or Cd^{2+} binding affects cyt *c* oxidation by H_2O_2 is discussed.

EXPERIMENTAL PROCEDURES

Sample Preparations. Horse heart and tuna cyt *c* were purchased from Sigma (St Louis, MO) and used without further purification. The purity of the commercial cyt *c* preparation was determined using denaturing protein gel electrophoresis. Cyt *c* was dissolved in a Tris-hydroxymethylaminomethane (Tris)/NaCl buffer: 50 mM Tris-HCl at pH 7.2 and 25 mM NaCl.

For the analysis of cyt *c* oxidation by H_2O_2, a 2 mM cyt *c* solution was reduced using 6 mM dithionite. Excess dithionite was removed by filtration through a PD-10 column (Amersham Bioscience) equilibrated with the Tris/NaCl buffer freed from metals by incubation with chelex resin. For experiments performed in ^2H_2O, the Tris/NaCl buffer was dried using a speed-vacuum system and then dissolved in ^2H_2O. For each sample, 4 μL of a 1.5 mM solution of reduced cyt *c* was diluted in 980 μL of the deuterated buffer. $ZnCl_2$ was added from a concentrated solution in ^2H_2O, and the sample was incubated for 24 h at 15 °C. A total of 8 or 16 μL of a concentrated H_2O_2 solution (100 mM) was added to the sample to trigger the oxidation reaction.

For the analysis of ferrocyt *c* oxidation by H_2O_2, cyt *c* was used at ~6 μM concentration and H_2O_2 was used at

Scheme 1: Schematic View of the ATR Device with the Dialysis Membrane[a]

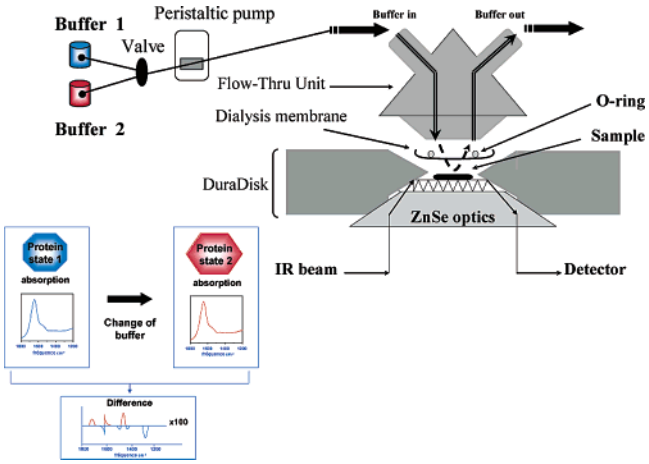

[a] The ATR device (*SensIr* Technologies) consists of a diamond crystal mounted in a stainless steel plate such that a 4.3 mm diameter surface is exposed for sample application. The IR beam is deflected in to and out of the prism by ZnSe optics, and the geometry is such that nine internal reflections occur at the prism surface on which the sample is blocked by the dialysis membrane as described in the Experimental Procedures. The flow-thru unit above the membrane allowed continuous perfusion of the solutions.

concentrations between 200 and 1600 μM. Cyt *c* concentrations were determined from reduced solutions using an extinction coefficient of 106 100 M^{-1} cm^{-1} at 410 nm (*52*). The oxidation kinetic of cyt *c* was monitored through the absorption change at 550 nm using a Cary 50 UV−vis spectrometer (Varian). The absorption at 550 nm was measured for 3 min. The initial slope was recorded. The rate constant of cyt *c* oxidation by H_2O_2 was determined from two kinetics recorded with two concentrations of H_2O_2, to avoid incidence from the low level of cyt *c* auto-oxidation (i.e., oxidation without H_2O_2). The influence of Zn^{2+} concentration on the cyt *c* oxidation kinetics was fitted assuming the same binding site for oxidized and reduced cyt *c*.

Microdialysis System Adapted for ATR−FTIR Spectroscopy. We used an ATR device from *SensIR* Technologies (CT) fitted with a 9 bounce diamond microprism with a 4.3 mm surface diameter and ZnSe optics (Scheme 1). This device is equipped with a flow-thru unit, which can be fixed above the ATR unit and allows the diffusion of solutions in a small chamber of approximately 30 μL above the diamond microprism.

The dialysis membrane (Spectra/Por membrane of MWCO: 6000−8000) was applied on the sample and maintained between the flow-thru unit and the diamond crystal using a 0.2 mm thick O ring (Scheme 1). Using solutions of known protein concentrations and comparing FTIR absorption spectra of samples recorded with or without the microdialysis setup, we determined that the dialysis membrane delimited a sample volume of 1−2 μL on the diamond crystal, corresponding to a sample thickness of less than 70 μm (not shown). A 2 μL aliquot of the 5 mM cyt *c* solution was deposited on the diamond window. The absorption of the sample reached 0.8 absorption units at the maximum absorption at 1640 cm^{-1}. The flow-thru unit was connected via silicone tubing (1.6 mm diameter, MasterFlex, Vernon Hills, IL) to a peristaltic pump (Pump drive PD5201 Heidolph) and to an electronically controlled three-way valve (Amersham Pharmaciabiotech). The peristaltic pump regulated the flow rate to 1−2 mL/min. With this flow rate, a delay of 1 h was necessary for the first equilibration of the sample in the ATR microdialysis chamber, before starting the measurements. This first equilibration delay was determined by absorption differences calculated from successive FTIR spectra recorded on the sample. Thereafter, a delay of 5−6 min was optimized after each change in buffer before the recording of the FTIR difference spectra. A three-way valve monitored through the FTIR spectrometer was used to select the buffer flowing through the microdialysis−ATR setup as described in refs *23*, *25*, and *26*. A program was developed to synchronize FTIR data acquisition with the diffusion of the buffers through the sample.

Oxidoreduction of Cyt c. Direct electrochemistry of cyt *c* was performed essentially as described in ref *16*, using the same electrochemical cell and a 4 μm thick gold mesh as a working electrode (Buckbee Mears, MN). The working electrode was surface-modified by dipping it for 5 min in a 5 mM pyridine-3-carboxaldehyde thiosemi-carbazone (PATS-3, purchased from Lancaster) solution heated to 80−90 °C. Excess PATS-3 was thoroughly removed with 18 MΩ Millipore water. The experiments were performed with a 5 mM cyt *c* solution in 50 mM Tris at pH 7.2 with 100 mM KCl as a supporting electrolyte. The reference electrode consisted in an Ag/AgCl/KCl (3M) system (E_m = 208 mV/NHE). The potential was applied to the three-electrodes system cell using an EG&G (model 362) potentiostat, controlled by the FTIR spectrometer. To analyze the effect of Zn binding on the redox properties of cyt *c*, ferrocyt *c* at 150 μM was incubated in the Tris/NaCl buffer containing 0.4 mM $ZnCl_2$ and then concentrated to ~1 mM using a microconcentrator (Amicon). Direct electrochemistry was performed, as electrochemistry in the presence of the following redox mediators: ferricyanide, *N*,*N*,*N*′,*N*′-tetramethyl-paraphenylene-diamine (TMPD), diaminodurene, *p*-benzoquinone, 2,5-dimethyl *p*-benzoquinone, 1,2-naphthoquinone, phenazine methosulfate, and duroquinone. The redox mediators were at 40 μM final concentration.

For the chemical oxidation and reduction of cyt *c* performed using the ATR−FTIR setup coupled to the microdialysis system, cyt *c* was equilibrated by the continuous flow of the Tris/NaCl buffer containing 5 mM potassium ferricyanide. When the FTIR absorption spectrum of the sample had stabilized, a single-beam spectrum was recorded (reference spectrum) and the flowing solution was switched to a Tris/NaCl buffer containing 2 mM TMPD and 0.5 mM dithionite. The buffers were degassed and flushed with argon. In these conditions, cyt *c* was reduced within 5 min. Typically, one reduction−oxidation cycle lasted for 20 min: the acquisition time per spectrum lasted ~5 min, and two spectra were recorded sequentially after equilibration of the sample with the reducing or oxidizing buffer. The spectra shown correspond to an average of 45 reductive or oxidative cycles of measurement.

Analysis of the Zn^{2+}− and Cd^{2+}−Cyt c Interactions Using the ATR−FTIR Microdialysis Setup. A total of 2 μL of a 5 mM cyt *c* solution (horse or tuna) was deposited on the diamond crystal. Sample equilibration was performed by the continuous flow of the metal-free Tris/NaCl buffer. When the FTIR sample absorption was stable (i.e., after ~60 min),

a single-beam spectrum was recorded and then the flowing solution was switched to the buffer containing either $ZnCl_2$ or $CdCl_2$. To avoid spectral changes because of slight variations in pH between the metal-free and metal-bearing solutions, the same buffer was divided in two parts and the pH was carefully adjusted after addition of $CdCl_2$ or $ZnCl_2$.

A delay of 6 min was chosen as a compromise between equilibration of the sample and spectral stability. For buffers with 2 mM Zn^{2+} or Cd^{2+} and more, the FTIR difference spectra did not change after 6 min of equilibration. For lower concentrations, this delay was not sufficient to reach a cyt *c*−Zn^{2+} (or Cd^{2+}) binding equilibration in the sample (see below). After this delay, a second single-beam spectrum corresponding to the "metal-bound" cyt *c* was recorded. The FTIR difference spectrum showing the absorption changes induced by the metal−cyt *c* interactions was obtained as the ratio of the two single-beam spectra "metal-bound" and "reference". The flowing solution was switched again to the metal-free buffer. After 6 min, the IR absorption changes indicated that Zn^{2+} (or Cd^{2+}) was successfully removed from the protein in solution. A total of 40 consecutive metal-binding cycles were accumulated for each sample. Results obtained with 2−5 samples were usually averaged to record FTIR difference spectra with high signal-to-noise.

FTIR Spectroscopy. The spectra were recorded, at 4 cm^{-1} resolution, on a Bruker IFS28 FTIR spectrometer equipped with a DTGS detector. All frequencies quoted have an accuracy of ±1 cm^{-1}. Typically, 300 interferograms were averaged for each single-beam spectrum.

NMR Spectroscopy. All of the spectra were recorded at 313 K on a Bruker Avance 500 spectrometer equipped with a triple resonance probe (^1H, ^{13}C, and ^{15}N). The heteronuclear experiments were conducted with natural abundance cyt *c* at a high concentration (5−8 mM). Using standard Bruker sequences, heteronuclear single-quantum correlation (HSQC) spectra were recorded in phase-sensitive mode in both dimensions using echo−antiecho time proportional phase incrementation (TPPI)-gradient selection. ^1H-^{15}N HSQC spectra were acquired with 320 transients, spectral windows of 16/40 ppm in the proton/nitrogen dimensions, and the carrier set at the water frequency and 118 ppm, respectively. ^1H-^{13}C HSQC spectra were acquired with 96 transients, spectral windows of 16/40 ppm in the proton/carbon dimensions, and the carrier set at the water frequency and 130 ppm, respectively. Magnetization transfers were optimized for a coupling constant of 200 Hz (*53*). No carbon decoupling was applied during acquisition. The relaxation delay used was 1 s, and a matrix of 2K × 96 points was acquired and transformed to 2K × 512 points after shifted sin-square multiplication. Analysis of the spectra was performed in part using SPARKY (T. D. Goddard and D. G. Kneller, University of California, San Franscisco, CA).

In the first experiments, the binding studies were performed in the same conditions as for FTIR, by adding $ZnCl_2$ on cyt *c* in 50 mM Tris at pH 7 and 50 mM NaCl. However, the use of a high concentration of $ZnCl_2$ required for the heteronuclear experiments prevented a careful pH adjustment of the solution. Addition of dilute NaOH led to zinc precipitation. Instead of $ZnCl_2$, $Zn(acetate)_2$ was successfully used in 200 mM potassium acetate as buffer at pH 7 in the subsequent experiments. Even in these conditions, a small precipitation of the zinc ion was observed during the long acquisition time required for the 2D heteronuclear experiments.

RESULTS

The first report on the use of a dialysis system coupled to ATR−FTIR spectroscopy concerned the analysis of protein−protein interactions, involving the membrane-protein rhodopsin deposited as a thin layer on the ATR internal reflection element (IRE). Upon diffusion of effectors, large IR changes were detected at the level of peptide amide I (peptide $\nu_{C=O}$) and amide II [$\nu_{C=N} + \delta(NH)$] IR modes, which were analyzed as the dissociation of protein−protein or protein−membrane interactions (*28*, *29*). We developed a new application of a dialysis system coupled to ATR−FTIR spectroscopy to extend this approach to the direct detection of changes at the molecular level on proteins in solution induced by chemicals diffused through the dialysis membrane.

IR changes as small as 10^{-4} absorption units are expected for the contribution of single vibrators in proteins. To reach this sensitivity, we decreased the equilibration time and increased the spectral quality by limiting the volume of the protein solution in contact with the IRE of the ATR accessory. We used an ATR device from *SensIR* Technologies fitted with a 9 bounce diamond microprism forming a 4.3 mm diameter circular surface exposed to the protein sample. A microdialysis cell of 1−2 μL, corresponding to a thickness of 70 μM was built on top of the diamond crystal using a dialysis membrane as described in the Experimental Procedures and illustrated in Scheme 1. Buffer solutions differing only by the presence of one reacting species were perfused alternately through this membrane in the protein sample, which consisted of an homogeneous concentrated protein solution above the diamond. After buffer exchange, a delay of 5−6 min was optimized for the equilibration of the protein solution before collecting the FTIR spectra.

Chemical Oxidation (Reduction) of Cyt c Using the ATR−FTIR Microdialysis System. The performance of the microdialysis system to detect minute changes in proteins was tested by monitoring the chemical reduction and oxidation of cyt *c* (Figure 1). Reproducible spectra corresponding to cyt *c* reduction (—) and reoxidation (- - -) were obtained by the alternate perfusion across the dialysis membrane of a Tris/NaCl buffer containing ferricyanide (oxidizing buffer) or TMPD and dithionite (reducing buffer), (Figure 1A, see the Experimental Procedures). Recording FTIR spectra at varying time after the buffer switch, we determined that cyt *c* reduction was achieved within 5 min in these conditions. The symmetry of the spectra recorded upon reduction and subsequent reoxidation of cyt *c* demonstrates that only IR bands associated to the redox reaction are observed in the spectra of Figure 1A.

The reduced minus oxidized spectrum of cyt *c* (—) is in full agreement with the difference spectrum previously obtained using electrochemistry coupled to FTIR spectroscopy (*16*, *43*, *54*) as demonstrated in Figure 1B. The only noticeable difference between spectra of Figure 1B is an increase in the relative intensity of bands with decreasing wavenumber values in the spectrum recorded with the microdialysis ATR−FTIR system. This is due to the reflection system, in which the penetration depth of the IR

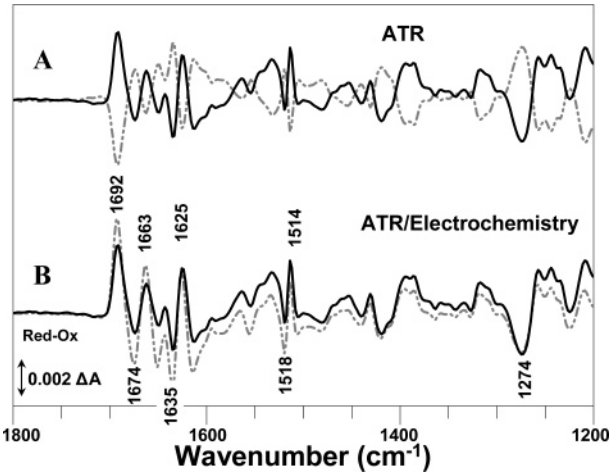

FIGURE 1: Comparison of difference spectra obtained with the microdialysis ATR−FTIR setup and with FTIR coupled to electrochemistry. (A) Reduced minus oxidized (—) and oxidized minus reduced (- - -) difference spectra of cyt *c* recorded using the ATR−FTIR setup coupled to the microdialysis system. (B) Comparison of reduced minus oxidized spectra of cyt *c* recorded using ATR−FTIR setup (—) and by FTIR coupled to electrochemistry (- - -). The spectra recorded using electrochemistry correspond to an average from 45 reductive or oxidative cycles.

evanescent wave dp depends on the wavelength λ according to the equation $dp = (\lambda/n_1)/(2\pi(\sin^2\theta - (n_2/n_1)^2)^{1/2}$, where n_1 and n_2 correspond to the refractive index of the diamond crystal and the protein solution, respectively, and θ is the incidence angle of the beam (*55* and references therein).

In the spectra of Figure 1, the largest band at 1692 cm^{-1} for reduced cyt *c* was assigned first to a β-strand structure (*56*) or to a heme propionic group (*16*). Recently, this band was assigned to a type-III β-turn structure that shifts to 1674 cm^{-1} for oxidized cyt *c* (*43*). The band at 1663 cm^{-1} was assigned to a type-II β-turn structure and signals at 1635 (ox) and 1625 (red) cm^{-1} to the weak portion of the β-strand structure of cyt *c* directly interacting with the heme propionates (*43*). On the basis of H/^{2}H exchange experiments, the bands at 1518 (ox) and 1514 (red) cm^{-1} were assigned to the ν_{19}(CC) ring mode of a tyrosine side chain (*16*). This shows that IR changes from individual vibrating groups are identified using the two FTIR difference techniques.

Identification of a Zn^{2+}- and Cd^{2+}-Binding Site in Cyt c. We observed that Zn^{2+} and Cd^{2+} selectively inhibit ferrocyt *c* oxidation by H_2O_2. Ferrocyt *c* is oxidized by H_2O_2 with a rate constant of 0.8−0.9 M^{-1} s^{-1} (*51*). We measured the oxidation kinetics of ferrocyt *c* with increasing concentrations of H_2O_2, in the absence or presence of Zn^{2+} (Figure 2A). The plots of Figure 2A are in accordance with a bimolecular reaction both in the absence or presence of Zn^{2+}. The plots do not go through the zero intercept. This is due to a residual oxidation of ferrocyt *c* in the absence of H_2O_2, which could be explained by the presence of oxygen or metal traces in the solution. Rate constants of 0.6 and 0.33 M^{-1} s^{-1} in the absence or presence of Zn^{2+}, respectively, were calculated from data in Figure 2A. We reproducibly observed in different measurement series that Zn^{2+} reduced the rate constant of cyt *c* oxidation by almost a factor of 2 (Figure 2A and Table 1).

The rate of ferrocyt *c* oxidation was then followed as a function of Zn^{2+} concentration (Figure 2B, ●). The experimental points could be fitted assuming the presence of a

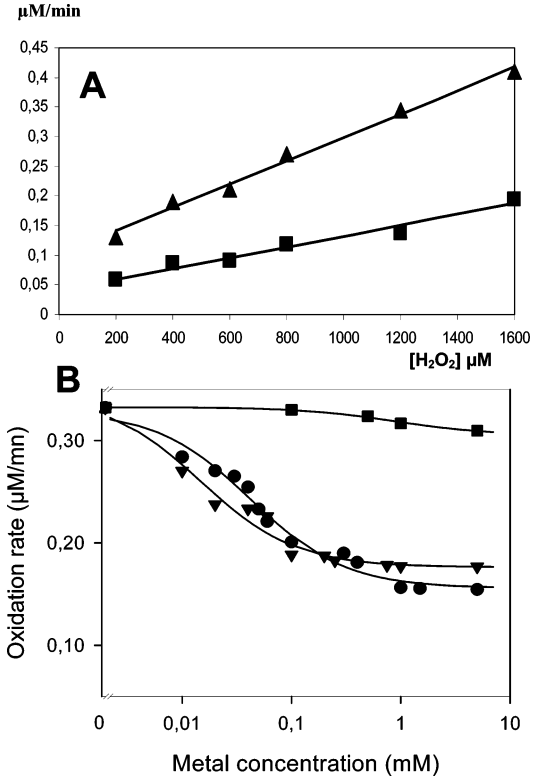

FIGURE 2: Influence of Zn^{2+} and Cd^{2+} on the rate of ferrocyt *c* oxidation by H_2O_2. (A) Rate of oxidation of ferrocyt *c* (6 μM) by H_2O_2 as a function of H_2O_2 concentration, in the absence (▲) or presence (■) of 1 mM $ZnCl_2$. The rate was measured by the absorption change at 550 nm typical for ferrocyt *c*. (B) Semilogarithmic representation of the influence of increasing Zn^{2+} (●), Cd^{2+} (▼), or Mg^{2+} (■) concentration on the initial rate of ferrocyt *c* (6 μM) oxidation by H_2O_2 (800 μM H_2O_2). The experimental points were fitted (—) assuming the presence of a metal-binding site both for reduced and oxidized cyt *c*, oxidation rates of 0.15 and 0.17 μM min^{-1} for Zn^{2+}- and Cd^{2+}-bound cyt *c*, respectively, and dissociation constants of 17 and 42 μM.

Table 1: Effect of H/^{2}H Exchange on the Oxidation Rate of Cyt *c* by H_2O_2

	H_2O	^2H_2O	$k(H_2O)/k(^2H_2O)$
0 mM Zn	$k = 0.97$ M^{-1} s^{-1}	$k = 0.18$ M^{-1} s^{-1}	5.4
0.4 mM Zn	$k = 0.46$ M^{-1} s^{-1}	$k = 0.07$ M^{-1} s^{-1}	6.6
k(0 mM Zn)/ k(0.4 mM Zn)	2.1	2.7	

binding site for Zn^{2+} identical for both reduced and oxidized cyt *c*, characterized by a dissociation constant of 42 μM (—). The presence of this binding site for both reduced and oxidized cyt *c* was indeed demonstrated using FTIR and NMR spectroscopy (see below). A similar effect on the oxidation kinetics of cyt *c* was observed with Cd^{2+} (Figure 2B, ▼), and the data were fitted with a curve indicating a dissociation constant of 17 μM. In contrast, the oxidation rate of cyt *c* was only slightly affected by increasing concentrations of $MgCl_2$ (■) up to 50 mM $MgCl_2$ (not shown).

To better understand the mechanism by which Zn^{2+} affects the oxidation kinetics of ferrocyt *c* by H_2O_2, we analyzed the impact of Zn^{2+} on the effect of H/^{2}H exchange on the rate of ferrocyt *c* oxidation. The rate constant of ferrocyt *c* oxidation by H_2O_2 was 5.4 times smaller for ferrocyt *c* incubated in a ^2H_2O buffer for 24 h as compared to samples incubated in H_2O during the same period (Table 1). In the

presence of $ZnCl_2$, the oxidation rate constant was 6.6 times smaller in ^2H_2O than in H_2O (Table 1). These data suggest that the oxidation of ferrocyt *c* involves proton rearrangements within the protein that are affected by Zn^{2+} binding.

The UV−vis absorption spectrum of reduced or oxidized cyt *c* remained unchanged in the presence of Zn^{2+}, and the EPR spectrum of oxidized cyt *c* remained characteristic of a low spin state at pH 7.5, with up to 5 mM $ZnCl_2$ (applied to a 1 mM cyt *c* solution, not shown). This indicated that Zn^{2+} did not perturb the immediate vicinity of the heme iron. Cyclic voltammetry performed in the thin-layer electrochemical cell designed for FTIR spectroscopy indicated that the midpoint potential of the heme iron was not significantly altered by the presence of Zn^{2+} with 53 ± 5 mV (versus Ag/AgCl/3M KCl) as compared to free cyt *c* (46 mV, not shown, *16*).

Collectively, these data indicate that there is a Cd^{2+}- and Zn^{2+}-binding site in cyt *c*, at a distance from the heme that alters the oxidation kinetics of ferrocyt *c* by H_2O_2.

Zn^{2+} Binding to Cyt c. We used the ATR−FTIR microdialysis system to identify the binding site of Zn^{2+} or Cd^{2+} in cyt *c*. A 5 mM solution of ferrocyt *c* was perfused with the Tris/NaCl buffer containing 100 μM dithionite. FTIR absorption spectra of the sample were recorded before and after switching from this metal-free buffer to the same buffer containing 2 mM $ZnCl_2$. The difference spectrum calculated from these two absorption spectra, denoted "Zn^{2+} minus free", is shown Figure 3A (− −). The positive bands are those that appear upon perfusion of cyt *c* with the Zn-containing buffer, while the negative bands are those that are suppressed by the interaction with Zn. The spectral changes were a maximum of 6 min after buffer exchange. They could be reversed by the subsequent perfusion of the metal-free buffer (Figure 3A, - - -). Very similar FTIR difference spectra were obtained upon Zn^{2+} binding to reduced or oxidized cyt *c* (parts A and B of Figure 3). This indicates that the interactions of Zn^{2+} and cyt *c* are the same for reduced and oxidized cyt *c*. For convenience, oxidized cyt *c* was used for the following FTIR experiments.

The Zn^{2+} minus free spectrum presents a small number of IR bands with amplitudes ranging from 10^{-4} to 5.10^{-4} absorbance units. These bands were reproducibly observed with different samples. They correspond to IR modes of individual amino acid side chains and peptide groups of cyt *c* involved in the structural changes associated with the Zn^{2+}−cyt *c* interaction. The simultaneous occurrence of positive bands at 1609−1600 and 1429 cm^{-1} on one hand and of negative bands at 1549 and 1398 cm^{-1} on the other hand strongly suggests that the Zn^{2+}−cyt *c* interactions involve side chain(s) of Asp and/or Glu amino acids. Indeed, the signals at 1609−1600 and 1549 cm^{-1} are in the typical frequency range of the $\nu_{as}(COO^-)$ mode of carboxylates, while the bands at 1429 and 1398 cm^{-1} are in the corresponding $\nu_s(COO^-)$ mode frequency domain (*57*, *58*).

The signals at 1670 and 1649 cm^{-1} occur in the region where $\nu_{C=O}$ modes from peptide groups are expected to contribute (*59*). The small size of these signals indicates that only slight structural rearrangements occur at the level of the peptide backbone upon Zn^{2+}−cyt *c* interaction.

Of particular interest is the positive band at 1115 cm^{-1}. In this spectral region, IR modes from amino acid side chains are usually small and sensitive to $H_2O/^2H_2O$ exchange (*57*, *59*), except for a histidine ring mode, the $\nu_{C_5N\tau}$ IR mode,

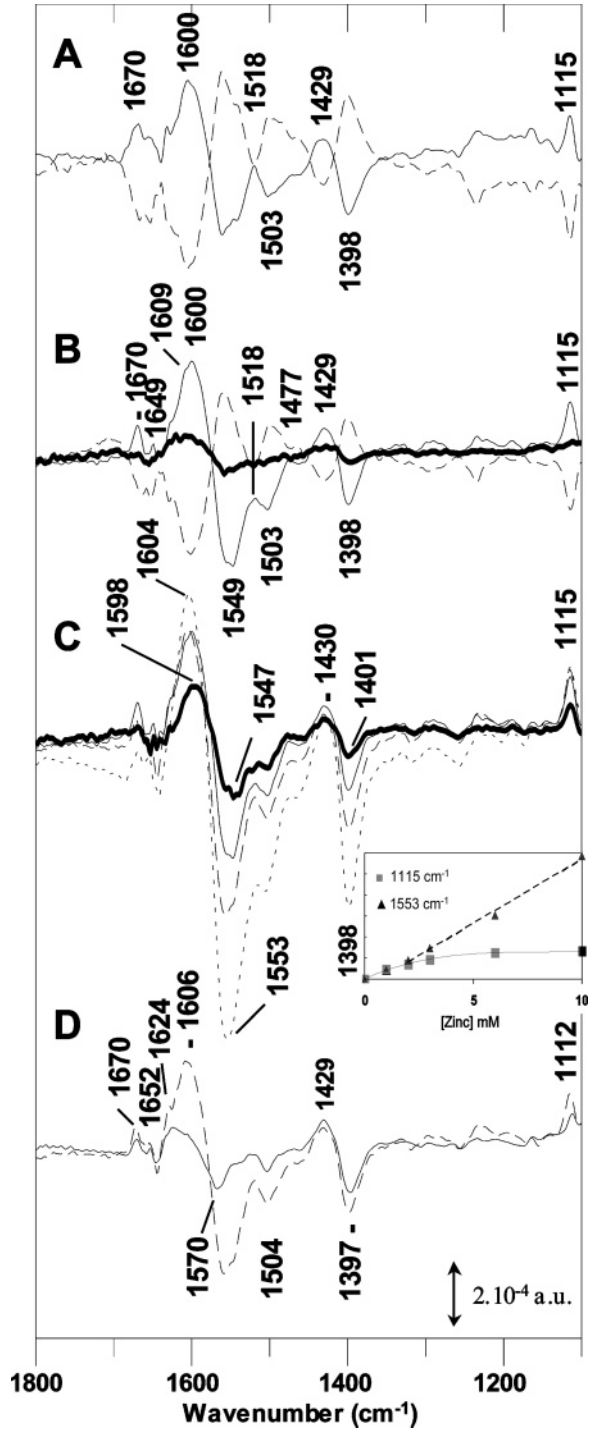

FIGURE 3: FTIR difference spectra corresponding to the interaction of Zn^{2+} with reduced cyt *c* (A) or oxidized cyt *c* (B, — and − − −). Spectra with a continuous line correspond to the Zn^{2+} minus free spectrum, and spectra with a dashed line correspond to the reverse reaction. The spectra are obtained by the alternate perfusion of the Tris/NaCl buffer with or without 2 mM $ZnCl_2$. The Mg^{2+} minus free spectrum recorded with oxidized cyt *c* with the Tris/NaCl buffer with or without 50 mM $MgCl_2$ is shown with a thick line in B. (C) Zn^{2+} minus free spectra recorded with the Tris/NaCl buffer containing 0.6 mM $ZnCl_2$ (—), 2 mM $ZnCl_2$ (—, same as — in B), 3 mM $ZnCl_2$ (- - -), and 6 mM $ZnCl_2$ (···). (Inset) IR band intensity at 1115 and 1553 cm^{-1} as a function of the $ZnCl_2$ concentration in the Tris/NaCl buffer. (D) Comparison of the Zn^{2+} minus free (- - -) and Cd^{2+} minus free (—) FTIR difference spectra recorded with oxidized cyt *c*.

which is enhanced upon coordination to metals and was observed in various proteins (*60*−*68*) and model spectra (*64*). The presence of this signal strongly supports that a histidine side chain of cyt *c* coordinates Zn^{2+}.

Effect of Mg^{2+} on Cyt c. The FTIR difference spectrum recorded upon cyt *c* perfusion with the Tris/NaCl buffer containing 50 mM $MgCl_2$ is shown in Figure 3B, —. It contrasts with that recorded with $ZnCl_2$, because it only shows IR bands at 1605/1560 and ≃1420/1400 cm^{-1}, characteristic for carboxylate groups. There is no specific effect of Mg^{2+} on the oxidation kinetics of ferrocyt *c* by H_2O_2 (Figure 2B), and we assign these IR difference bands to the side chains of Glu or Asp located at the cyt *c* surface, which are sensitive to electrostatic interactions with Mg^{2+}.

Effect of Zn^{2+} Concentration on the IR Bands. To discriminate the effect of specific binding and of electrostatic interactions at the protein surface, we analyzed the influence of Zn^{2+} concentration on the "Zn^{2+} minus free" FTIR difference spectra (Figure 3C), for concentrations ranging from 0.6 to 6 mM. It was not possible to obtain reliable data with Zn^{2+} concentrations lower than 0.6 mM. Data in Figure 3C show that the amplitude of a number of IR bands including the positive bands at 1115 and 1670 cm^{-1} saturate with increasing $ZnCl_2$ concentrations (inset of Figure 3C). This behavior corresponds to chemical groups involved in a specific interaction with Zn^{2+}, at a Zn^{2+}-binding site. The intensity of other IR bands, notably negative ones at ≃1580−1500 and 1398 cm^{-1}, further increased with Zn^{2+} concentration, with an almost linear dependence. These bands are in the frequency range of ν_{as} and $\nu_s(COO^-)$ IR modes. A closer analysis of the carboxylate $\nu_{as}(COO^-)$ IR range shows that the position of both the positive and negative bands vary with increasing Zn^{2+} concentration. At 0.6 mM Zn^{2+}, the bands are at a maximum at 1598 and 1547 cm^{-1} (—), while these maxima appear at 1604 and 1553 cm^{-1} for the curve recorded with 6 mM $ZnCl_2$ (···).

We interpret the IR data as the occurrence of one carboxylate group at the Zn^{2+}-binding site, characterized by ν_{as} and $\nu_s(COO^-)$ IR modes at 1598 and 1430 cm^{-1} in the presence of Zn^{2+} (and at 1547 and 1401 cm^{-1} in absence of Zn^{2+}) and the implication of additional carboxylate modes, characterized by IR changes at ≃1604−1553 and 1430−1398 cm^{-1}, associated to glutamate side chains at the cyt *c* surface, forming nonspecific electrostatic interactions with the increasing Zn^{2+} concentration in the buffer (*40*). Similar carboxylate IR bands are the only ones identified in the "Mg^{2+} minus free" spectrum recorded with cyt *c* (Figure 3B, —).

The amplitude dependence of the IR bands as a function of the Zn^{2+} concentration is not in accordance with the dissociation constant (42 μM) deduced from the effect of the Zn^{2+} concentration on the oxidation kinetics of ferrocyt *c* by H_2O_2. This may be rationalized by the fact that the FTIR sample consists of 1−2 μL of a highly concentrated solution of cyt *c* (2−5 mM). For experiments using buffers with low Zn^{2+} concentrations, large perfusion delays are required to reach the Zn^{2+}−cyt *c* binding equilibrium. These delays are not compatible with the acquisition of high-quality FTIR difference spectra. The FTIR−microdialysis approach is thus not optimum to determine metal-binding constants but gives specific information on the chemical nature of the metal ligands.

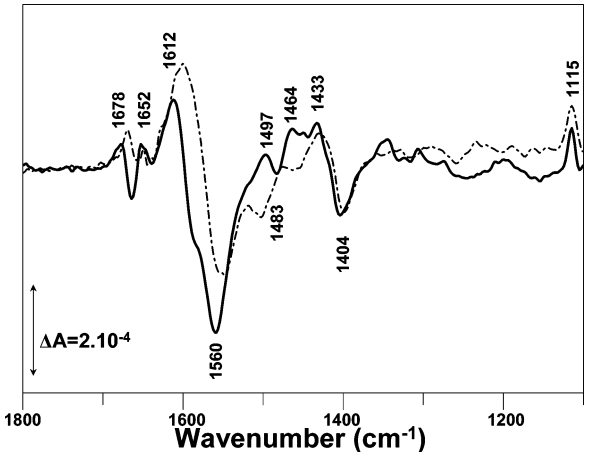

FIGURE 4: Zn^{2+} minus free FTIR difference spectra recorded with cyt *c* in ^2H_2O (—) and in H_2O (- · -).

Scheme 2: Structural Model of Cyt *c*[a]

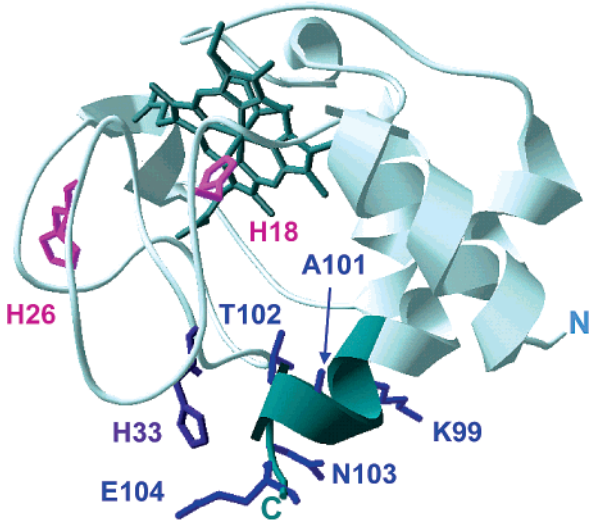

[a] The drawing was generated with Swiss-PdbViewer, from the PDB file 1HRC (*85*). Changes in the properties of His 33 and the amino acids colored in blue and purple have been detected upon Zn^{2+} binding using FTIR and NMR spectroscopy.

Cd^{2+}−Cyt c Interaction. The Cd^{2+}−cyt *c* interaction gives rise to FTIR difference spectra similar to those obtained upon the Zn^{2+}−cyt *c* interaction (Figure 3D, —), supporting that Cd^{2+} and Zn^{2+} bind at the same site in cyt *c*. Bands at 1670, 1652, 1504, 1429, 1397, and 1112 cm^{-1} are within a few wavenumbers from those observed upon Zn^{2+} binding. The signal at 1112 cm^{-1} is assigned to the IR side-chain mode of one histidine ligand of Cd^{2+}. The bands at 1606 and 1429 cm^{-1} are best assigned to the ν_{as} and $\nu_s(COO^-)$ IR modes of a carboxylate ligand of Cd^{2+}. These modes contribute at 1570 and 1397 cm^{-1} in the absence of Zn^{2+}.

$H_2O/^2H_2O$ Exchange: Assignment of the IR Modes. To obtain more precise assignments for the bands observed in the "Zn^{2+} minus free" FTIR difference spectrum, we analyzed the effect of $H_2O/^2H_2O$ exchange on that spectrum. The ν_{as} and $\nu_s(COO^-)$ IR modes of carboxylate groups hydrogen bonded to water molecules are expected to shift to slightly higher frequencies in ^2H_2O (*59*, *69*, *70*). This behavior was also observed for carboxylate ligands of metals (*71* and references therein). The bands at 1598, 1549, 1430, and 1401 cm^{-1} in H_2O (Figure 3B) are shifted to 1612, 1560,

Scheme 3: Comparison of the Amino Acid Sequences of Horse and Tuna Heart Cyt *c*

```
Horse : 1 gdvekgkkif vqkcaqchtv ekggkhktgp nlhglfgrkt gqapgftytd anknkgitwk
Tuna  : 1 gdvakgkktf vqkcaqchtv enggkhkvgp nlwglfgrkt gqaegysytd ankskgivwn

Horse : 61 eetlmeylen pkkyipgtkm ifagikkkte redliaylkk atne
Tuna  : 61 ndtlmeylen pkkyipgtkm ifagikkkge rqdlvaylks ats
```

1433, and 1404 cm^{-1} in ^2H_2O (Figure 4) in support of their assignment to hydrogen-bonded carboxylate ν_{as} and $\nu_s(COO^-)$ IR modes.

The band at 1115 cm^{-1} is not sensitive to $H_2O/^2H_2O$ exchange. This rules out any contribution from hydroxyl groups at this frequency and supports the assignment of this band to the $\nu_{C_5N\tau}$ IR ring mode of an histidine-chelating Zn^{2+}. Indeed, we have shown using methylimidazole (MeIm), that the MeIm $\nu_{C_5N\tau}$ IR mode is largely enhanced and upshifted from 1104 to 1113 cm^{-1} upon Zn^{2+} complexation (*64*). We do not detect the small negative band expected at 1104 cm^{-1} in the "Zn^{2+} minus free" spectrum probably because this small signal is hidden below the positive band at 1115 cm^{-1}. The $\nu_{C_4C_5}$ ring mode of histidine is expected at 1605 or 1586 cm^{-1} for Zn−histidine complexes, depending on the imidazole nitrogen involved in the metal coordination (*64*). This weak mode is hidden below the stronger absorption bands of the carboxylate group(s).

Three histidines are present in horse heart cyt *c*. His 18 is coordinated to the heme iron, while His 26 and His 33 are closer to the protein surface (Scheme 2). We exclude an interaction of Zn^{2+} with the heme ligand His 18 because Zn^{2+} does not perturb the midpoint potential nor electronic and EPR spectra of cyt *c*. His 26 is not located at proximity from Glu or Asp side chains in horse heart cyt *c* and therefore is not a plausible candidate for the Zn^{2+}-binding site. His 33 is situated near the side chain of Glu 104 at the C terminus of horse heart cyt *c* (Scheme 2), and we propose from the FTIR data that the Zn^{2+}-binding site involves His 33 and Glu 104.

Tuna Cyt c. To test this hypothesis, we analyzed the effect of Zn^{2+} binding to the cyt *c* from tuna, a natural cyt *c* variant, where Glu 104 is lacking and His 33 is substituted by a tryptophan (Schemes 2 and 3). The "Zn^{2+} minus free" FTIR difference spectrum recorded with tuna cyt *c* by the perfusion of Tris/NaCl buffer with or without 2 mM $ZnCl_2$ is displayed in Figure 5 (—). This spectrum is dominated by IR changes of carboxylate groups. The signals observed at 1670, 1649, 1503, 1257, and 1115 cm^{-1} in horse heart cyt *c* are absent. The lack of the positive band at 1115 cm^{-1} confirms that this signal is due to Zn^{2+}-bound His 33 and that the Zn^{2+}-binding site in horse heart cyt *c* involves His 33 and Glu 104 at the C terminus. The ν_{as} and $\nu_s(COO^-)$ IR modes observed in the spectrum recorded with tuna cyt *c* are assigned to conserved Glu at the protein surface in non-specific electrostatic interactions with Zn^{2+}.

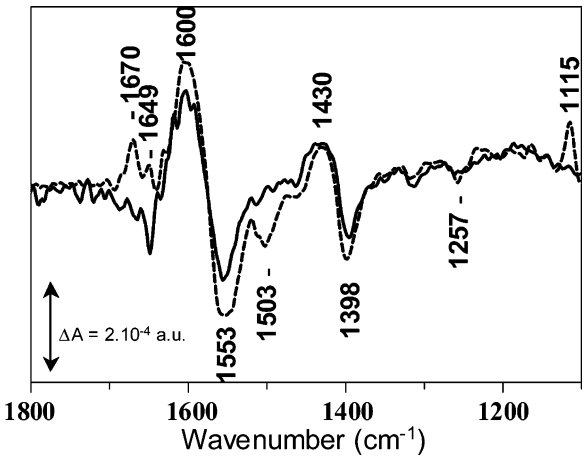

FIGURE 5: Zn^{2+} minus free FTIR difference spectra recorded with cyt *c* from tuna heart (—) and cyt *c* from horse heart (- - -).

NMR Spectroscopy of the Cyt c−Zn^{2+} Interaction. ^1H-^{13}C (^{15}N) HSQC spectra of cyt *c* in both redox states were acquired in absence and presence of 10 equiv of zinc acetate. Zinc acetate was preferred because it allows a more efficient control of the pH when compared to $ZnCl_2$. No significant changes were observed however in the 1D spectra recorded with the two salts. The overall spectra recorded with and without Zn^{2+} display only minor changes, which is in good agreement with localized structural modifications associated with metal binding. For ^1H-^{13}C HSQC spectra, portions of

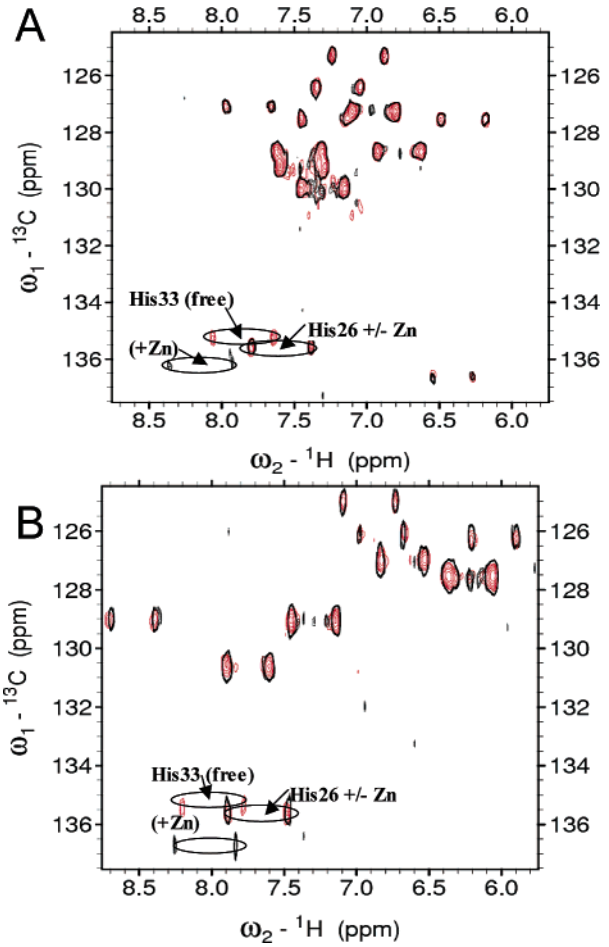

FIGURE 6: Dual ^1H-^{13}C HSQC spectra of reduced (A) and oxidized (B) cyt *c* in the absence (red) or presence (black) of 10 equiv of Zn^{2+}.

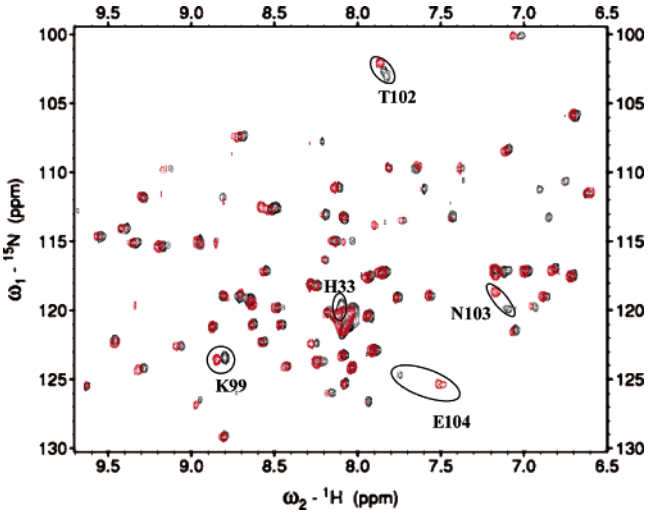

FIGURE 7: Dual ^{1}H-^{15}N HSQC spectra of oxidized cyt *c* in the absence (red) and presence (black) of 10 equiv of Zn−acetate.

the spectra acquired with a delay optimized for a large coupling constant of 200 Hz (*53*) are shown in Figure 6. This coupling constant is typical for resonances of histidine imidazole side chains. As expected, in the spectra acquired without decoupling during the acquisition period, two doublets with large $^1J_{CH}$ couplings appear downfield of the phenylalanine signals, observed below 132 ppm in the ^{13}C dimension, and are assigned to the two ^{1}H-^{13}C resonances of His 26 and His 33, on the basis of previously reported ^{1}H data on oxidized and reduced cyt *c* (*72*−*76*). In the presence of zinc, in the oxidized state, the doublet assigned to His 33 was shifted from 7.66/135.57 to 8.02/137.0 ppm, whereas the equivalent cross-peak of His 26 was not modified (Figure 6A). A similar behavior was observed in the reduced state, with a significant shift of the ^{1}H-^{13}C cross-peak of His 33 from 7.83/135.39 to 8.02/137.0 ppm (Figure 6B). These spectra demonstrate that the imidazole ring of His 33 is involved in zinc binding in both oxidation states.

To get a more complete description of the residues involved in zinc binding, ^{1}H-^{15}N HSQC have been realized in both redox states with and without zinc acetate. All of the 2D spectra were recorded at 313 K, in favor of the narrowing of the resonances. This shortened the acquisition time but at the expense of the absence of signals from some NH groups experiencing fast exchange with water at this temperature. Nevertheless, most of the cross-peaks already assigned for cyt *c* are observed in the spectra (*72*). Figure 7 shows ^{1}H-^{15}N HSQC of oxidized cyt *c* with and without Zn^{2+}. These spectral modifications caused by Zn^{2+} addition are indicative of the changes in chemical shifts of the peptide NH groups upon Zn^{2+} addition. The major changes are labeled. The ^{1}H-^{15}N cross-peak of His 33 is only slightly modified, indicating that the zinc coordination, involving the imidazole side chain, does not induce a structural change at the level of the histidine peptide group. The most important shift variations are encountered for the ^{1}H-^{15}N cross-peaks of Glu 104, Asn 103, Thr 102, and Lys 99. The C-terminal region is flexible, and the NMR data are characteristic for a rearrangement of this region of cyt *c* induced by Zn^{2+} binding. On the basis of the extent of the chemical-shift difference, the Glu 104 appears to be the major residue involved in Zn^{2+} complexation, in agreement with the detection of a carboxylate metal ligand using the ATR−FTIR approach.

DISCUSSION

A Zn^{2+}/Cd^{2+}-Binding Site in Cyt c. In this work, we have demonstrated that the microdialysis setup coupled to ATR−FTIR spectroscopy allows the detection at the molecular level of structural changes associated with the change in redox state of cyt *c*. The quality of the data is equivalent to that obtained by spectroelectrochemistry. Moreover, we show that this technique permits the investigation of metal-binding sites in proteins, by the perfusion of buffers with or without the metal. Various metal sites are in principle accessible to this technique, for all kinds of metals and for soluble or membrane-bound proteins. Here, we precisely describe a Zn^{2+}- and Cd^{2+}-binding site in cyt *c* that affects its reactivity toward hydrogen peroxide.

We obtained reproducible FTIR difference spectra using the microdialysis ATR setup for the interaction of cyt *c* with Zn^{2+} or Cd^{2+} and showed that part of these signals is associated with a specific binding site in the protein. While the FTIR microdialysis approach is not optimum for an accurate determination of the metal-binding constants, it gives specific information on the chemical nature of the metal ligands. We concluded that the Zn^{2+}- or Cd^{2+}-binding site in horse heart cyt *c* comprises a histidine and a carboxylate. Inspection of the cyt *c* amino acid sequence suggested that the binding site involved His 33 and Glu 104. This was supported by the comparison of data recorded with horse heart cyt *c* and tuna cyt *c*, lacking these two residues.

The comparison of the HSQC ^{1}H-^{13}C NMR data recorded with reduced and oxidized cyt *c* alone or in the presence of 10 equiv of Zn^{2+} clearly demonstrated that the chemical shifts for the His 33 side chain are specifically and largely affected by Zn^{2+}, while His 26 remains unchanged. The HSQC ^{1}H-^{15}N data further showed that the peptide NH group of His 33 is slightly affected, indicating that Zn^{2+} binding is not accompanied by a large structural change at the level of the peptide bond, which is engaged in a type-II β-turn structure. The peptide NH group of Glu 104 at the C terminus is subjected to a large change, in agreement with the involvement of its side chain in Zn^{2+} coordination, as proposed from the FTIR data. Concomitantly, changes were observed for the peptide backbone of surrounding residues Ala 103, Thr 102, and Lys 99 (Figure 7) that are indicative of a conformational change at the C terminus upon zinc binding. Similar results were observed for the Zn^{2+} interaction with reduced or oxidized cyt *c*.

The use in combination of these two techniques shows the efficiency of the microdialysis ATR−FTIR difference spectroscopy approach to characterize metal-binding sites in proteins. The effect of Zn concentration on the FTIR spectra demonstrated that a carboxylate and a histidine side chain were involved in a specific binding site, while other carboxylates at the protein surface were involved in electrostatic interactions with the metal salts in solution. The FTIR data were sustained by the analysis by 2D NMR, and the NMR data further showed that Zn binding also involved a slight structural change at the C terminus. The microdialysis ATR−FTIR method needs small quantities of proteins and gives information on the chemical nature of the metal ligands.

It is not limited to specific metals and can be extremely useful in the absence of X-ray structures or NMR data. In this respect, the use of the microdialysis system for the analysis of complex membrane proteins such as transporters is a very attractive perspective.

Mechanisms by which Zn Binding Affects the Oxidation Kinetics of Cyt c by H_2O_2. The kinetic of cyt *c* oxidation by H_2O_2 is largely affected by $H/^2H$ exchange, which is due primarily to the rupture of O−H bonds in the substrate. The fact that Zn^{2+} affects both the cyt *c* oxidation kinetics by H_2O_2 and the effect of $H/^2H$ exchange on these kinetics further suggests that these reactions also involve proton reorganization within cyt *c*, which are altered upon Zn^{2+} binding. While the oxidation of cyt *c* in solution is not limited by proton rearrangements, interaction of cyt *c* with a coated electrode surface modifies the redox-induced structural changes within cyt *c* (*43*) and the rate of cyt *c* oxidation can become limited by proton reorganization within the protein (*44*). Also, a solvent deuterium isotope effect on the reduction thermodynamics of cyt *c* was reported recently (*77*), which was interpreted as an oxidation-state-dependent hydrogen bonding within the hydration sphere of the protein.

These data suggest that the Zn^{2+}-binding site, although remote from the heme iron, affects the oxidation kinetics of cyt *c* by perturbing a redox-sensitive hydrogen-bonding network in the protein. Zn^{2+} and Cd^{2+} were shown to interact with proton-transfer chains or hydrogen-bonding networks in a number of proteins, including the bacterial photosynthetic reaction centers (*78*, *79*), the mitochondrial bc_1 complex (*80*−*82*), and cytochrome *c* oxidase (*83*).

The C terminus of cyt *c* is not known to participate in a hydrogen-bonding network that varies upon the change in the redox state of cyt *c*. In contrast, the peptide bonds of His 33, Leu 32, and Asn 31 participate in a hydrogen-bond network that extends to the heme propionate 7 and Tyr 48 (*85*). His 33, Asn 31, and the propionate 7 are among the most displaced residues upon cyt *c* oxidation, as seen by NMR (*40*, *41*, *73*, *75*, *84*). The binding of Zn^{2+} or Cd^{2+} at His 33 may perturb the hydrogen-bonding network and/or create an electrostatic barrier that hinders proton reorganization within this network during ferrocyt *c* oxidation by H_2O_2.

Finally, the dissociation constants of 17 and 42 μM observed for Cd^{2+} and Zn^{2+} suggest that partial cyt *c*−Cd^{2+} or −Zn^{2+} binding may occur in mitochondria following a Cd^{2+} or Zn^{2+} stress. Cd^{2+} is a highly toxic metal, and its toxicity is notably associated with oxidative stress and alterations of the mitochondria (*86*−*88*). Partial inhibition of complexes II and III was recently reported for Cd^{2+} concentrations ranging from 10 to 20 μM, together with a significant increase in the production of reactive oxygen species (*88*).

Contradictory roles have been assigned in the literature for the oxidation of cyt *c* by H_2O_2. A protective role against oxidative stress has been associated with the ability of cyt *c* to scavenge hydrogen peroxide (*89*). In contrast, a prooxidant role has been assigned to the reaction of cyt *c* with H_2O_2, when cyt *c* is closely associated to the mitochondria membrane. Cyt *c* reactivity toward H_2O_2 is greatly enhanced upon association with phosphatydilserine or cardiolipin (*32*, *90*). In these conditions, oxidized cyt c behaves as a peroxidase that leads to the peroxidation of lipids, especially cardiolipin (*32*, *90*). A role in signaling of the lipid peroxide thus formed was proposed (*32*). This peroxidation reaction was also proposed to trigger cyt *c* release from its close association to the mitochondria membrane, a reaction that may initiate apoptosis (*31*, *91*, *92*). The impact of Cd^{2+} or Zn^{2+} on cyt *c* properties when associated to phospholipids of the mitochondria membrane should now be investigated to evaluate precisely a possible role as pro- or antioxidant in the mitochondria.

ACKNOWLEDGMENT

We acknowledge Alain Boussac for the low-temperature EPR spectra on cyt *c*, Jérôme Lavergne for helpful discussions and comments on the manuscript, and André Verméglio for his support to this project.

REFERENCES

1. Hartwig, A., Asmuss, M., Ehleben, I., Herzer, U., Kostelac, D., Pelzer, A., Schwerdtele, T., and Bürkle, A. (2002) Interference by toxic metal ions with DNA repair processes and cell cycle control: Molecular mechanisms, *Environ. Health Perspect. 110*, 797−799.
2. Leonard, S. S., Harris, G. K., and Shi, X. (2004) Metal-induced oxidative stress and signal transduction, *Free Radical Biol. Med. 37*, 1921−1942.
3. Busenlehner, L. S., Pennella, M. A., and Giedroc D. P. (2003) The SmtB/ArsR family of metalloregulatory transcriptional repressors: Structural insights into prokaryotic metal resistance, *FEMS Microbiol. Rev. 27*, 131−143.
4. Luk, E., Jensen, L. T., and Culotta, V. C. (2003) The many highways for intracellular trafficking of metals, *J. Biol. Inorg. Chem. 8*, 803−809.
5. Kirk, M. L., and Peariso, K., (2003) Recent applications of MCD spectroscopy to metalloenzymes, *Curr. Opin. Chem. Biol. 7*, 220−227.
6. Solomon, E. I., Szilagyi, R. K., DeBeer George, S., and Basumallick, L. (2004) Electronic structures of metal sites in proteins and models: Contributions to function in blue copper proteins, *Chem. Rev. 104*, 419−458.
7. Ubbink, M., Worrall, J. A. R., Canters, G. W., Groenen E. J. J., and Huber, M. (2002) Paramagnetic resonance of biological metal centers, *Annu. Rev. Biophys. Biomol. Struct. 31*, 393−422.
8. Spiro, T. G., Czernuszewicz, R. S. (1995) Resonance Raman spectroscopy of metalloproteins, *Methods Enzymol. 246*, 416−460.
9. Hashimoto, S., Ono, K., and Takeuchi, H. (1998) UV resonance Raman scattering from metal-coordinating histidine residues in Cu,Zn-superoxide dismutase, *J. Raman Spectrosc. 29*, 969−975.
10. Wang, D., Zhao, X., Vargek, M., and Spiro, T. G. (2000) Metal-bound histidine modes in UV resonance Raman spectra of Cu, Zn superoxide dismutase, *J. Am. Chem. Soc. 122*, 2193−2199.
11. Mäntele, W. (1993) Reaction-induced infrared difference spectroscopy for the study of protein function and reaction mechanisms, *Trends Biochem. Sci. 18*, 197−202.
12. Siebert, F. (1995) Infrared spectroscopy applied to biochemical and biological problems, *Methods Enzymol. 246*, 501−526.
13. Heberle, J. (2000) Proton-transfer reactions across bacteriorhodopsin and along the membrane, *Biochim. Biophys. Acta 1458*, 135−144.
14. Nabedryk, E. (1996) In *Infrared Spectroscopy of Biomolecules* (Mantsch, H. H., and Chapman, D., Eds.) John Wiley and Sons, New York, pp 39−81.
15. Noguchi, T., and Berthomieu, C. (2004) Vibrational spectroscopy applied to the study of photosystem II in *Photosystem II: The Water/Plastoquinone Oxido-Reductase of Photosynthesis* (Wydrzynski, T., and Satoh, K., Eds.) Kluwer Academic, Dordrecht, The Netherlands, chapter 15, in press.
16. Moss, D., Nabedryk, E., Breton, J., and Mäntele, W. (1990) Redox-linked conformational changes in proteins detected by a combination of infrared spectroscopy and protein electrochemistry. Evaluation of the technique with cytochrome *c*, *Eur. J. Biochem. 187*, 565−572.

17. Gerwert, K. (1999) Molecular reaction mechanisms of proteins monitored by time-resolved FTIR spectroscopy, *Biol. Chem. 380*, 931−935.
18. Zscherp, C., and Barth, A. (2001) Reaction-induced infrared difference spectroscopy for the study of protein reaction mechanisms, *Biochemistry 40*, 1875−1883.
19. Marrero, H., and Rothschild, K. J. (1987) Conformational changes in bacteriorhodopsin studied by infrared attenuated total reflection, *Biophys. J. 52*, 629−635.
20. Fringeli, U. P., Apell, H. J., Fringeli, M., and Lauger, P. (1989) Polarized infrared absorption of Na^+/K^+-ATPase studied by attenuated total reflection spectroscopy, *Biochim. Biophys. Acta 984*, 301−312.
21. Ryan, S. E., Demers, C. N., Chew, J. P., and Baenziger, J. E. (1996) Structural effects of neutral and anionic lipids on the nicotinic acetylcholine receptor. An infrared difference spectroscopy study, *J. Biol. Chem. 271*, 24590−24597.
22. Ryan, S. E., Hill, D. G., and Baenziger, J. E. (2002) Dissecting the chemistry of nicotinic receptor−ligand interactions with infrared difference spectroscopy, *J. Biol. Chem. 277*, 10420−10426.
23. Iwaki, M., Andrianambinintsoa, S., Rich, P., and Breton, J. (2002) Attenuated total reflection Fourier transform infrared spectroscopy of redox transitions in photosynthetic reaction centers: Comparison of perfusion- and light-induced difference spectra, *Spectrochim. Acta 58*, 1523−1533.
24. Iwaki, M., Giotta, L., Akinsiku, A. O., Schagger, H., Fisher, N., Breton, J., and Rich, P. R. (2003) Redox-induced transitions in bovine cytochrome bc_1 complex studied by perfusion-induced ATR−FTIR spectroscopy, *Biochemistry 42*, 11109−11119.
25. Rich, P. R., and Breton, J. (2001) FTIR studies of the CO and cyanide adducts of fully reduced bovine cytochrome *c* oxidase, *Biochemistry 40*, 6441−6449.
26. Rich, P. R., and Breton, J. (2002) Attenuated total reflection Fourier transform infrared studies of redox changes in bovine cytochrome *c* oxidase: Resolution of the redox Fourier transform infrared difference spectrum of heme a(3), *Biochemistry 41*, 967−973.
27. Grimard, V., Li, C., Ramjeesingh, M., Bear, C. E., Goormaghtigh, E., and Ruysschaert, J.-M. (2004) Phosphorylation-induced conformational changes of cystic fibrosis transmembrane conductance regulator monitored by attenuated total reflection−Fourier transform IR spectroscopy and fluorescence spectroscopy, *J. Biol. Chem. 279*, 5528−5536.
28. Fahmy, K. (1998) Binding of transducin and transducin-derived peptides to rhodopsin studies by attenuated total reflection−Fourier transform infrared difference spectroscopy, *Biophys. J. 75*, 1306−1318.
29. Lehmann, N., Aradhyam, G. K., and Fahmy, K. (2002*)* Suramin affects coupling of rhodopsin to transducin, *Biophys. J. 82*, 793−802.
30. Capaldi, R. A., Darley-Usmar, V., Fuller, S., and Millett, F. (1982) Structural and functional features of the interaction of cytochrome *c* with complex III and cytochrome *c* oxidase, *FEBS Lett. 138*, 1−7.
31. Liu, X., Kim, C. N., Yang, J., Jemmerson, R., and Wang, X. (1996) Induction of apoptotic program in cell-free extracts: Requirement for dATP and cytochrome *c*, *Cell 86*, 147−157.
32. Kagan, V. E., Borisenko, G. G., Tyurina, Y. Y., Tyurin, V. A., Jiang, J., Potapovich, A. I., Kini, V., Amoscato, A. A., and Fujii, Y. (2004) Oxidative lipidomics of apoptosis: Redox catalytic interactions of cytochrome *c* with cardiolipin and phosphatidylserine, *Free Radical Biol. Med. 37*, 1963−1985.
33. Hagen, S. J., Latypov, R. F., Dolgikh, D. A., and Roder, H. (2002) Rapid intrachain binding of histidine-26 and histidine-33 to heme in unfolded ferrocytochrome *c*, *Biochemistry 41*, 1372−1380.
34. Chang, I. Jy., Lee, J. C., Winkler, J. R., and Gray, H. (2003) The protein-folding speed limit: Intrachain diffusion times set by electron-transfer rates in denatured $Ru(NH_3)_5$(His-33)-Zn-cytochrome *c*, *Proc. Nat. Acad. Sci. U.S.A. 100*, 3838−3840.
35. Maneg, O., Malatestab, F., Ludwig, B., and Drosou V. (2004) Interaction of cytochrome *c* with cytochrome oxidase: Two different docking scenarios, *Biochim. Biophys. Acta 1655*, 274−281.
36. Chevance, S., Le Rumeur, E., de Certaines, J. D., Simonneaux, G., and Bondon, A. (2003) ^{1}H NMR structural characterization of the cytochrome *c* modifications in a micellar environment, *Biochemistry 42*, 15342−15351.
37. Jemmerson, R., Liu, J., Hausauer, D., Lam, K. P., Mondino, A., and Nelson, R. D. (1999) A conformational change in cytochrome *c* of apoptotic and necrotic cells is detected by monoclonal antibody binding and mimicked by association of the native antigen with synthetic phospholipid vesicles, *Biochemistry 38*, 3599−3609.
38. Cortese, J. D., Voglino, A. L., and Hackenbrock, C. R. (1998) Multiple conformations of physiological membrane-bound cytochrome *c*, *Biochemistry 37*, 6402−6409.
39. Tuominen, E. K., Wallace, C. J., and Kinnunen, P. K. (2002) Phospholipid−cytochrome *c* interaction: Evidence for the extended lipid anchorage, *J. Biol. Chem. 277*, 8822−8826.
40. Feng, Y. Q., Roder, H., and Englander, S. W. (1990) Redox-dependent structure change and hyperfine nuclear magnetic resonance shifts in cytochrome *c*, *Biochemistry 29*, 3494−3504.
41. Feng, Y., and Englander, S. W. (1990) Salt-dependent structure change and ion binding in cytochrome *c* studied by two-dimensional proton NMR, *Biochemistry 29*, 3505−3509.
42. Bertini, I., Turano, P., Vasos, P. R., Bondon, A., Chevance, S., and Simonneaux, G. (2004) Cytochrome *c* and SDS: A molten globule protein with altered axial ligation, *J. Mol Biol. 336*, 489−496.
43. Ataka, K., and Heberle, J. (2004) Functional vibrational spectroscopy of a cytochrome *c* monolayer: SEIDAS probes the interaction with different surface-modified electrodes, *J. Am. Chem. Soc. 126*, 9445−9457.
44. Murgida, D. H., Hildebrandt, P., Wie, J., He, Y.-F., Liu, H., Waldeck, D. H. (2004) Surface-enhanced resonance Raman spectroscopic and electrochemical study of cytochrome *c* bound on electrodes through coordination with pyridinyl-terminated self-assembled monolayers, *J. Phys. Chem. B 108*, 2261−2269.
45. Iwahashi, H., Nishizaki, K., and Takagi, I. (2002) Cytochrome c catalyses the formation of pentyl radical and octanoic acid radical from linoleic acid hydroperoxide, *Biochem. J. 361*, 57−66.
46. Radi, R., Sims, S., Cassina, A., and Turrens, J. F. (1993) Roles of catalase and cytochrome *c* in hydroperoxide-dependent lipid peroxidation and chemiluminescence in rat heart and kidney mitochondria, *Free Radical Biol. Med. 15*, 653−659.
47. Jiang, J. Serinkan, B. F., Tyurina, Y. Y., Borisenko, G. G., Mi, Z., Robbins, P. D., Schroit, A. J., and Kagan V. E. (2003) Peroxidation and externalization of phosphatidylserine associated with release of cytochrome *c* from mitochondria, *Free Radical Biol. Med. 35*, 814−825.
48. Chance, B., Sies, H., and Boveris, A. (1979) Hydroperoxide metabolism in mammalian organs, *Physiol. Rev. 59*, 527−605.
49. Nishimura, G., Proske, R. J., Doyama, H., and Higuchi, M. (2001) Regulation of apoptosis by respiration: Cytochrome *c* release by respiratory substrates, *FEBS Lett. 505*, 399−404.
50. Petrosillo, G., Ruggiero, F. M., and Paradies G. (2003) Role of reactive oxygen species and cardiolipin in the release of cytochrome *c* from mitochondria, *FASEB J. 17*, 2202−2208.
51. Turrens, J. J., and McCord, J. M. (1988) How relevant is the reoxidation of ferrocytochrome *c* by hydrogen peroxide when determining superoxide anion production? *FEBS Lett. 227*, 43−46.
52. Margoliash, E., and Frohwirt, N. (1959) Spectrum of horse-heart cytochrome *c*, *Biochem. J. 71*, 570−572.
53. Pelton, J. G., Torchia, D. A., Meadow, N. D., and Roseman, S. (1993) Tautomeric states of the active-site histidines of phosphorylated and unphosphorylated IIIGlc, a signal-transducing protein from *Escherichia coli*, using two-dimensional heteronuclear NMR techniques, *Protein Sci. 2*, 543−558.
54. Schlereth, D. D., and Mantele, W. (1993) Electrochemically induced conformational changes in cytochrome *c* monitored by Fourier transform infrared difference spectroscopy: Influence of temperature, pH, and electrode surfaces, *Biochemistry 32*, 1118−1126.
55. Goormaghtigh, E., Raussens, V., and Ruysschaert, J.-M. (1999) Attenuated total reflection infrared spectroscopy of proteins and lipids in biological membranes, *Biochim. Biophys. Acta 1422*, 105−185.
56. Calvert, J. F., Hill, J. L., and Dong, A. (1997) Redox-dependent conformational changes are common structural features of cytochrome *c* from various species, *Arch. Biochem. Biophys. 346*, 287−293.
57. Venyaminov, S. Y., and Kalnin, N. N. (1990) Quantitative IR spectrophotometry of peptide compounds in water (H_2O) solutions. I. Spectral parameters of amino acid residue absorption bands, *Biopolymers 30*, 1243−1257.

58. Deacon, G. B., and Phillips, R. J. (1980) Relationships between the carbon−oxygen stretching frequencies of carboxylato complexes and the type of carboxylate coordination, *Coord. Chem. Rev. 33*, 227−250.
59. Venyaminov, S. Y., and Kalnin, N. N. (1990) Quantitative IR spectrophotometry of peptide compounds in water (H_2O) solutions. II. Amide absorption bands of polypeptides and fibrous proteins in α-, *β*-, and random coil conformations, *Biopolymers 30*, 1259−1271.
60. Berthomieu, C., Boussac, A., Mäntele, W., Breton, J., and Nabedryk, E. (1992) Molecular changes following oxidoreduction of cytochrome *b*559 characterized by Fourier transform infrared difference spectroscopy and electron paramagnetic resonance: Photooxidation in photosystem II and electrochemistry of isolated cytochrome *b*559 and iron protoporphyrin IX-bisimidazole model compounds, *Biochemistry 31*, 11460−11471.
61. Berthomieu, C, and Hienerwadel, R. (2001) Iron coordination in photosystem II: Interaction between bicarbonate and the QB pocket studied by Fourier transform infrared spectroscopy, *Biochemistry 40*, 4044−4052.
62. Berthomieu, C., Dupeyrat, F., Fontecave, M., Vermeglio, A., and Niviere, V. (2002) Redox-dependent structural changes in the superoxide reductase from *Desulfoarculus baarsii* and *Treponema pallidum*: A FTIR study, *Biochemistry 41*, 10360−10368.
63. Breton, J., Xu, W., Diner, B. A., and Chitnis, P. R. (2002) The two histidine axial ligands of the primary electron donor chlorophylls (P700) in photosystem I are similarly perturbed upon P700+ formation, *Biochemistry 41*, 11200−11210.
64. Dupeyrat, F., Vidaud, C., Lorphelin, A., and Berthomieu, C. (2004) Long distance charge redistribution upon Cu,Zn-superoxide dismutase reduction: Significance for dismutase function, *J. Biol. Chem. 279*, 48091−48101.
65. Hienerwadel, R., and Berthomieu, C. (1995) Bicarbonate binding to the non-heme iron of photosystem II investigated by Fourier transform infrared difference spectroscopy and ^{13}C-labeled bicarbonate, *Biochemistry 34*, 16288−16297.
66. Noguchi, T., Inoue, Y., and Tang, X.-S. (1999) Hydrogen bonding interaction between the primary quinone acceptor QA and a histidine side chain in photosystem II as revealed by Fourier transform infrared spectroscopy, *Biochemistry 38*, 399−403.
67. Schmidt, B., Hillier, W., McCracken, J., and Ferguson-Miller, S. (2004) The use of stable isotopes and spectroscopy to investigate the energy transducing function of cytochrome *c* oxidase, *Biochim. Biophys. Acta 1655*, 248−255.
68. Hasegawa, K., Ono, T.-A., and Noguchi, T. (2002) *Ab initio* density functional theory calculations and vibrational analysis of zinc-bound 4-methylimidazole as a model of a histidine ligand in metalloenzymes, *J. Phys. Chem. A 106*, 3377−3390.
69. Chirgadze, Y. N., Fedorov, O. V., and Trushina, N. P. (1975) Estimation of amino acid residue side-chain absorption in the infrared spectra of protein solutions in heavy water, *Biopolymers 14*, 679−694.
70. Maeda, A., Sasaki, J., Shichida, Y., Yoshizawa, T., Chang, M., Ni, B., Needleman, R., and Lanyil, J. K. (1992) Structures of aspartic acid-96 in the L and N intermediates of bacteriorhodopsin: Analysis by Fourier transform infrared spectroscopy, *Biochemistry 31*, 4684−4690.
71. Noguchi, T., Ono, T., and Inoue, Y. (1995) A carboxylate ligand interacting with a water molecule bound to the Mn-cluster in the oxygen-evolving center of photosystem II as revealed by Fourier transform infrared spectroscopy, *Biochim. Biophys. Acta 1228*, 189−200.
72. Liu, W., Rumbley, J., Englander, S. W., and Wand, A. J. (2003) Backbone and side-chain heteronuclear resonance assignments and hyperfine NMR shifts in horse cytochrome *c*, *Protein Sci. 12*, 2104−2108.
73. Banci, L., Bertini, I., Gray, H. B., Luchinat, C., Reddig, T., Rosato, A., and Turano P. (1997) Solution structure of oxidized horse heart cytochrome *c*, *Biochemistry 36*, 9867−9877.
74. Feng, Y., Roder, H., Englander, S. W., Wand, A. J., and Di Stefano, D. L. (1989) Proton resonance assignments of horse ferricytochrome *c*, *Biochemistry 28*, 195−203.
75. Banci, L., Bertini, I., Huber, J. G., Spyroulias, G. A., and Turano, P. (1999) Solution structure of reduced horse heart cytochrome *c*, *J. Biol. Inorg. Chem. 4*, 21−31.
76. Wand, A. J., Di Stefano, D. L., Feng, Y. Q., Roder, H., and Englander, S. W. (1989) Proton resonance assignments of horse ferrocytochrome *c*, *Biochemistry 28*, 186−194.
77. Battistuzzi, G., Borsari, M., Ranieri, A., and Sola, M. (2004) Solvent-based deuterium isotope effects on the redox thermodynamics of cytochrome *c*, *J. Biol. Inorg. Chem. 9*, 781−787.
78. Paddock, M. L., Graige, M. S., Feher, G., and Okamura, M. Y. (1999) Identification of the proton pathway in bacterial reaction centers: Inhibition of proton transfer by binding of Zn^{2+} or Cd^{2+}, *Proc. Natl. Acad. Sci. U.S.A. 96*, 6183−6188.
79. Axelrod, H. L., Abresch, E. C., Paddock, M. L., Okamura, M. Y., and Feher, G. (2000) Determination of the binding sites of the proton-transfer inhibitors Cd^{2+} and Zn^{2+} in bacterial reaction centers, *Proc. Natl. Acad. Sci. U.S.A. 97*, 1542−1547.
80. Berry, E. A., Zhang, Z., Bellamy, H. D., and Huang, L. (2000) Crystallographic location of two Zn^{2+}-binding sites in the avian cytochrome bc_1 complex, *Biochim. Biophys. Acta 1459*, 440−448.
81. Skulachev, V. P., Chistyakov, V. V., Jasaitis, A. A., and Smirnova, E. G. (1967) Inhibition of the respiratory chain by zinc ions, *Biochem. Biophys. Res. Commun. 26*, 1−6.
82. Link, T. A., and von Jagow, G. (1995) Zinc ions inhibit the Q_P center of bovine heart mitochondrial bc_1 complex by blocking a protonatable group, *J. Biol. Chem. 270*, 25001−25006.
83. Aagaard, E., Namslauer, A., and Brzezinski, A. P. (2002) Inhibition of proton transfer in cytochrome *c* oxidase by zinc ions: Delayed proton uptake during oxygen reduction, *Biochim. Biophys. Acta 1555*, 133−139.
84. Liu, W., Rumbley, J., Englander, W., and Wand, J. (2003) Backbone and side-chain heteronuclear resonance assignments and hyperfine NMR shifts in horse cytochrome *c*, *Protein Sci. 12*, 2104−2108.
85. Bushnell G. W., Louie, G. V., and Brayer, G. D. (1990) High-resolution three-dimensional structure of horse heart cytochrome *c*, *J. Mol. Biol. 214*, 585−595.
86. Hassoun, E., and Stohs, S. J. (1996) Cadmium-induced production of superoxide anion and nitric oxide, DNA single strand breaks, and lactate dehydrogenase leakage in J774A1 cell cultures, *Toxicology 112*, 219−226.
87. Koizumi, T., Yokota, T., Shirakura, H., Tatsumoto, H., and Suzuki, K. T. (1994) Potential mechanism of cadmium-induced cytotoxicity in rat hepatocytes: Inhibitory action of cadmium on mitochondrial respiratory activity, *Toxicology 92*, 115−125.
88. Wang, Y., Fang, J., Leonard, S., and Rurali Krishna Rao, K. (2004) Cadmium inhibits the electron-transfer chain and induces reactive oxygen species, *Free Radical Biol. Med. 36*, 1434−1443.
89. Zhao, Y., Wang, Z.-B., and Xu, J.-X. (2003) Effect of cytochrome *c* on the generation and elimination of $O_2^{-\cdot}$ and H_2O_2 in mitochondria, *J. Biol. Chem. 278*, 2356−2360.
90. Iwase, H.; Takatori, T.; Nagao, M.; Iwadate, K., and Nakajima, M. (1996) Monoepoxide production from linoleic acid by cytochrome *c* in the presence of cardiolipin, *Biochem. Biophys. Res. Comm. 222*, 83−89.
91. Shidoji, Y.; Hayashi, K.; Komura, S.; Ohishi, N., and K. Yagi (1999) Loss of molecular interaction between cytochrome *c* and cardiolipin due to lipid peroxidation, *Biochem. Biophys. Res. Comm. 264*, 343−347.
92. Jiang, J., Serinkan, B. F., Tyurina, Y. Y., and Bori, G. Y. (2003) Peroxidation and externalization of phosphatidylserine associated with release of cytochrome *c* from mitochondria, *Free Radical Biol. Med. 35*, 814−825.

BI050322L